A 3-D printed bandpass filter using tm-mode slotted spherical resonators with enhanced spurious suppression

Zhang, Fan; Guo, Cheng; Zhang, Yi; Gao, Yang; Liu, Bing; Shu, Minjie; Wang, Yi; Dong, Yuliang; Lancaster, Michael J.; Xu, Jun

DOI:
10.1109/ACCESS.2020.3040293

IEEE Access
Multidisciplinary | Rapid Review | Open Access Journal

Received November 11, 2020, accepted November 19, 2020, date of publication November 24, 2020,
date of current version December 9, 2020.

Digital Object Identifier 10.1109/ACCESS.2020.3040293

A 3-D Printed Bandpass Filter Using TM_{211}-Mode Slotted Spherical Resonators With Enhanced Spurious Suppression

FAN ZHANG[1,2], (Member, IEEE), CHENG GUO[3], YI ZHANG[1], (Student Member, IEEE), YANG GAO[4], (Member, IEEE), BING LIU[1], MINJIE SHU[3], YI WANG[2], (Senior Member, IEEE), YULIANG DONG[5], MICHAEL J. LANCASTER[2], (Senior Member, IEEE), AND JUN XU[1]

[1]School of Physics, University of Electronic Science and Technology of China, Chengdu 610054, China
[2]Department of Electronic, Electrical, and Systems Engineering, University of Birmingham, Birmingham B15 2TT, U.K.
[3]School of Information and Communications Engineering, Xi'an Jiaotong University, Xi'an 710049, China
[4]Department of Information Engineering, Zhengzhou University, Zhengzhou 450001, China
[5]Chengdu Aeronautic Polytechnic, Chengdu 610100, China

Corresponding authors: Jun Xu (xujun@uestc.edu.cn) and Yi Wang (y.wang.1@bham.ac.uk)

This work was supported in part by the National Natural Science Foundation of China under Grant 62001367, and in part by the U.K. Engineering and Physical Science Research Council under Contract EP/S013113/1. The work of Fan Zhang was supported in part by the China Scholarship Council through the State Scholarship Fund.

ABSTRACT This article presents a *Ka*-band fourth-order slotted spherical resonator waveguide bandpass filter (BPF) with a wide spurious suppression stopband. It uses the first higher-order TM_{211} mode rather than the fundamental TM_{101} mode of the spherical resonator in order to obtain a higher unload quality factor (Q_u) for smaller in-band insertion loss, as well as a larger filter volume that gives better tolerance to fabrication errors in high frequency applications. By introducing slots that interrupt surface currents, the fundamental TM_{101} and two higher spurious modes (TE_{101} and TM_{311}) can be suppressed without compromising the unloaded quality factor of the TM_{211} mode. In addition, the filter topology is optimized to further enhance the suppression level of the spurious passbands. A Z-shaped topology has been found effective in decreasing the coupling strength of the spurious TM_{311} mode. An analysis is performed to demonstrate the better tolerance of the Z-shaped filter over the conventional TM_{101}-mode spherical resonator filter. For verification, a fourth-order slotted spherical resonator waveguide BPF with a center frequency of 31 GHz and bandwidth of 880 MHz is designed and manufactured using a selective laser melting (SLM) 3-D printing process. The measured results show an average in-band insertion loss of 1.53 dB, and a passband return loss better than 13.6 dB. The stopband of the filter is extended up to 40.9 GHz with a rejection level greater than 20 dB.

INDEX TERMS Bandpass filter, slotted spherical resonator, TM_{211}, spurious suppression, selective laser melting, 3-D printed.

I. INTRODUCTION

Microwave waveguide bandpass filters (BPFs) play an essential role in current communication systems due to their advantages of low insertion loss and high-power handing capacity. Conventionally, waveguide BPFs using simple resonators such as rectangular and cylindrical shaped resonators [1], [2] are usually fabricated by conventional computer numerical controlled (CNC) milling. Over the past few years, 3-D printing (or additive manufacturing) has found increasing applications in microwave BPFs [3]–[13]. For example, [3] reported a filter based on super-ellipsoid resonators with excellent performance. In [6], quasi-elliptic filters were realized using mushroom-shaped resonators. Recently, spherical resonators have been shown to be suitable for 3-D printing [14]–[21], with ultra-low insertion loss due to the high Q_u of the printed resonators. However, they suffer from higher order modes that are close in

The associate editor coordinating the review of this manuscript and approving it for publication was Xiu Yin Zhang.

frequency to the fundamental TM_{101} mode, and this degrades the out of band performance of the filter. This problem has been investigated by using the rotated topology [14], the depressed super-ellipsoid cavity [3], and the slotted spherical resonators [20], [21].

TABLE 1. Comparison of three types of resonators.

	Q_u @ 31 GHz	Dimensions (mm)	Nearest spurious mode (GHz)	Volume (mm^3)
Rectangular	3423	7.112 × 3.556 × 6.6 (length)	47.13 (TE_{201})	167
Cylindrical	4818	3.23 (radius) × 10.16 (height)	35.57 (TE_{112})	333
Spherical @ TM_{101}	6215	4.2 (radius)	43.5 (TM_{2m1})	310
Spherical @ TM_{211}	7393	5.95 (radius)	36.1 (TE_{101})	882

Electrical conductivity of the cavity walls is assumed to be 3.56×10^7 S/m in the CST simulation.

On the other hand, as mentioned in [14], higher order modes of the spherical resonator offer higher Q_us than that of the fundamental TM_{101}. The increased volume may be a disadvantage at low frequencies, but a potential benefit for high frequency components where the large volume gives the filter a better tolerance to fabrication. In this work, the first higher-order TM_{211} mode is utilized to design filters. Table 1 compares the characteristics of three types of resonators (i.e., rectangular resonator, cylindrical resonator, and spherical resonator) resonating at 31 GHz. These include two spherical resonators working on the TM_{101} and TM_{211} modes. It is found that the TM_{211} mode has the highest Q_u. However, it suffers from a nearby spurious TE_{101}-mode at 36.1 GHz that would deteriorate its stopband performance.

In this article, a novel TM_{211}-mode slotted spherical resonator with suppressed spurious modes is proposed. Two approaches are applied to suppress the spurious resonances. Firstly, the fundamental TM_{101} mode and two higher spurious modes (TE_{101} and TM_{311}) are suppressed by slotting the spherical resonator diagonally and interrupting their surface currents. This results in a wide spurious-free stopband. The surface current of the TM_{211} mode is not interfered with and therefore its high Q_u is maintained. Secondly, the filter topology is optimized to increase the suppression level. The slotted spherical resonator filter arranged in an inline topology suffers from a relatively shallow suppression of the spurious passbands formed by the TE_{101} and TM_{311} modes. To overcome this problem, the geometrical configuration of the filter is arranged in a "Z" topology to achieve better spurious suppression by decreasing the coupling strength of the spurious TM_{311} mode. Compared with previous work on spherical resonators [14]–[21], the proposed new design concept based on high-order mode offers higher unload quality factor, and allows higher tolerance to fabrication, which is critically important for practical applications. Moreover, higher lower and upper spurious suppression can be achieved. It should be mentioned that the proposed slotted spherical resonator can also be utilized in other topologies, such as cascaded trisection (CT) filters, extracted pole filters, and canonical filters [22].

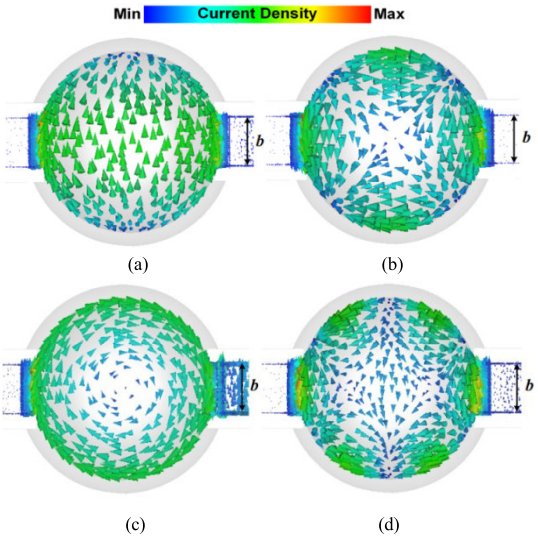

FIGURE 1. Simulated surface current distributions (side views) of resonant modes in a two-port weakly coupled air-filled spherical resonator. (a) TM_{101}; (b) TM_{211}; (c) TE_{101}; (d) TM_{311}. The parameter b represents the height of the feeding rectangular waveguide.

II. SLOTTED SPHERICAL RESONATORS

The first four resonant modes of a spherical resonator are the TM_{101}, TM_{211}, TE_{101}, and TM_{311} modes [14], [21], their simulated surface current distributions (side views) in a weakly coupled spherical resonator are shown in Fig. 1, while the corresponding top views of these modes can be found in our previous work [21]. Here the structure is fed by rectangular waveguides. The first higher TM_{211} mode at 31 GHz will be utilized to form the filter passband in this work. The fundamental TM_{101} and the spurious TE_{101} and TM_{311} are located at 22.0 GHz, 36.1 GHz, and 39.8 GHz, respectively. Our goal is to suppress the unwanted modes without decreasing the Q_u of the TM_{211} mode. This is achieved by introducing slots at the diagonal positions of the spherical resonator, as shown in Fig. 2(a). The slots are deliberately placed in parallel with the current induced by the TM_{211} mode so that it causes minimal disturbance at the TM_{211} frequency. However, for the other three modes (TM_{101}, TE_{101}, and TM_{311}), the slots intercept their current paths, and radiation will be generated. In addition, the slots are placed in the region with a small current density for the TM_{211} mode, but with relatively large current densities for the other three modes. Accordingly, without significantly interfering the TM_{211} mode, the TM_{101}, TE_{101}, and TM_{311} modes are suppressed via radiation. Fig. 2(b) shows the simulated transmission responses of the unslotted and slotted resonators fed with waveguides. The simulations are performed from Computer Simulation Technology (CST) Studio Suite [23].

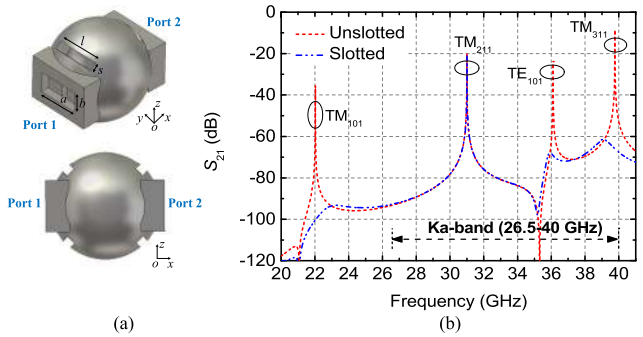

FIGURE 2. The proposed slotted spherical resonator with weak waveguide external couplings. Feeding windows of 1.5 mm × 3.556 mm are used. (a) A geometrical illustration (upper: A 3-D view; lower: A side view). (b) Simulated transmission coefficients. The electrical conductivity of 3.56×10^7 S/m was used in the simulation for cavity boundaries. The slot dimensions are $s = 1.30$ mm, $l = 10.8$ mm.

It is evident that the three spurious modes are effectively suppressed, while the TM_{211} mode is conserved.

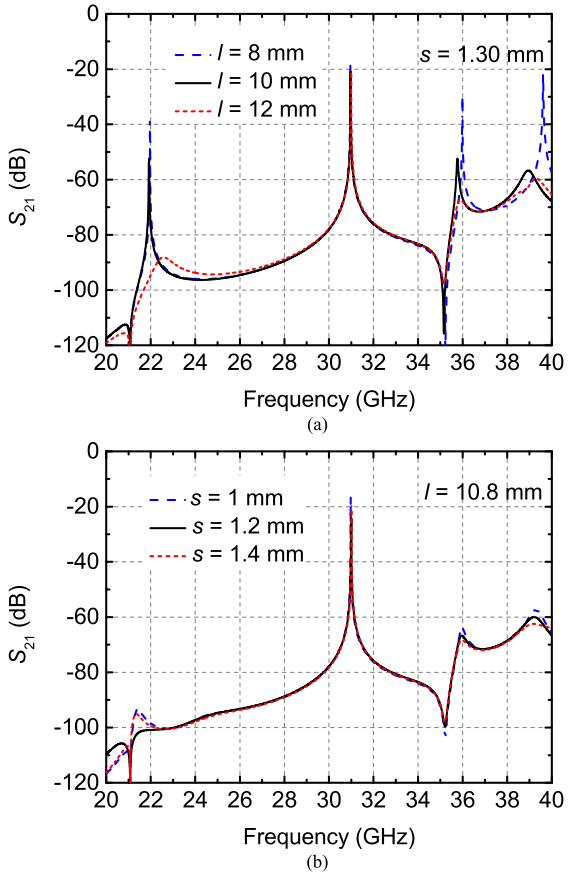

FIGURE 3. EM-simulated transmission responses of the slotted spherical resonator with different slot dimensions. (a) The transmission response against slot length *l*. (b) The transmission response against slot width *s*.

Fig. 3 shows the simulated transmission responses of the slotted spherical resonator against different slot dimensions. As it can be seen, slot length l plays the main role in suppressing the TM_{101}, TE_{101} and TM_{311} modes. Moreover, the suppression level on the TM_{101} mode is stronger than that on the TE_{101} and TM_{311} modes. With the increasing length l from 8 to 12 mm, the suppression level on the three modes is significantly enhanced, as shown in Fig. 3(a). This is because the current densities of the TM_{101}, TE_{101}, and TM_{311} modes are concentrated in the slotted region. The slot width s can also be utilized to increase the suppression level, as shown Fig. 3(b), but the effect is much weaker.

To confirm the slots do not have a significant impact on the Q_u of the TM_{211}-mode, the radiation quality factor (Q_r) of the TM_{211} mode can be found from simulation. The loaded quality factor (Q_L) can be calculated as

$$Q_L = f_0/\Delta f_{3dB} \tag{1}$$

where f_0 and Δf_{3dB} represent the resonant frequency and the 3-dB bandwidth with respect to the magnitude of S_{21} at f_0. From [22], the Q_L of the slotted spherical resonator in free space can be expressed as

$$Q_L^{-1} = Q_e^{-1} + Q_c^{-1} + Q_r^{-1} \tag{2}$$

where Q_e, Q_c, and Q_r are the external quality factor, conductor quality factor, and radiation quality factor, respectively. The unloaded quality factor (Q_u) can be expressed by Q_c and Q_r, i.e.,

$$Q_u^{-1} = Q_c^{-1} + Q_r^{-1} \tag{3}$$

In order to obtain Q_r due to the slots for the TM_{211} mode, we set the conductor making the sphere to be a perfect electrical conductor (PEC) to make Q_c infinite. To negate the effect of Q_e, a weakly coupled resonator as shown in Fig. 2(a) is simulated by making a very small coupling aperture (1.5 mm × 3.556 mm). Hence, the simulated Q_L was approximately equal to Q_r. It is found Q_r is around 3.5×10^6. Q_c is calculated by simulating the resonator again with conductor set as aluminum (using an electrical conductivity of 3.56×10^7 S/m). Q_c is founded to be around 7.12×10^3, which is much lower than the value of Q_r. This shows that the radiation loss caused by the slots is negligible.

Fig. 4 plots the calculated quality factors of the slotted spherical resonator for the TM_{211}-mode against various slot dimensions. In Fig. 4(a), as l increases from 4 to 12 mm, Q_c and Q_u are only reduced by less than 2.8%. Q_r is reduced by over 63% within the inspected region. Similarly, in Fig. 4(b), as s increases from 0.8 mm to 1.6 mm, Q_c and Q_u are reduced by less than 2.4%, and Q_r is reduced by over 45%. Both results in Fig. 4 indicate that the increased slot dimensions introduce negligible conductor loss for the resonator. The value of Q_r is much larger than Q_c, indicating very little radiation loss for the TM_{211} mode. It should be mentioned that the decreased Q_u of the TM_{211} mode within the inspected region is still much larger than that of the fundamental TM_{101} mode (i.e., 6215, as shown in Table 1).

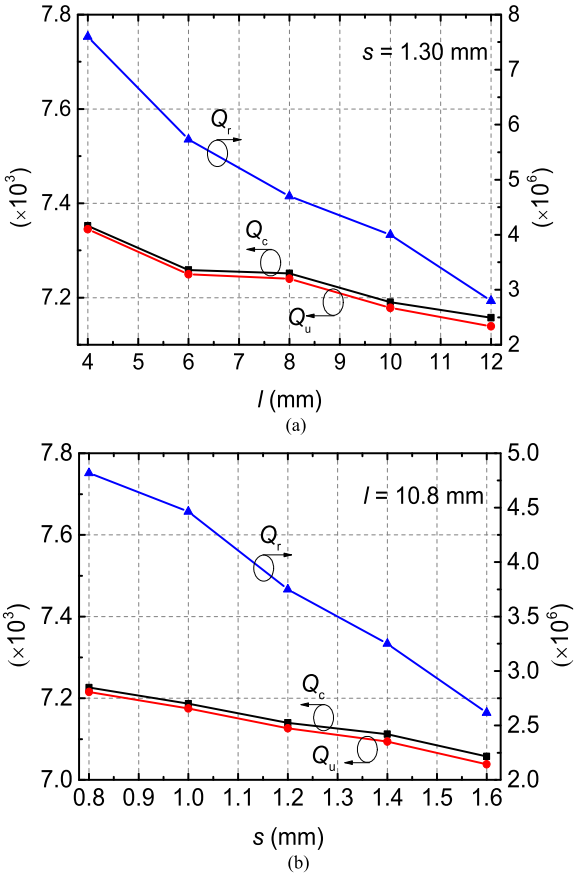

FIGURE 4. Simulated TM_{211}-mode quality factors of a slotted spherical resonator under different slot dimensions. (a) The quality factors versus slot width l. (b) The quality factors against slot length s.

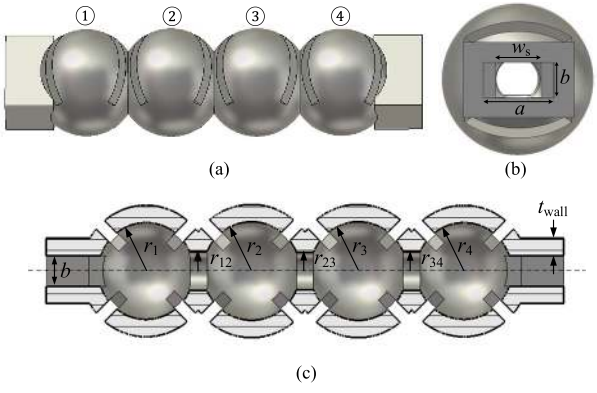

FIGURE 5. Illustration of the in-line fourth-order Ka-band BPF based on slotted spherical resonators. (a) A 3-D view. (b) A side view. (c) Cross section view. Critical dimensions of the filter in millimeters are $a = 7.112$, $b = 3.556$, $w_S = 4.58$, $r_1 = r_4 = 5.59$, $r_2 = r_3 = 5.69$, $r_{12} = r_{34} = 2.26$, $r_{23} = 2.16$, $t_{wall} = 2$. The slot dimensions of the resonators (s_i and l_i denoted in Fig. 1(a), i = 1, 2, 3, and 4 for the i^{th} resonator) are $s_1 = s_4 = 1.3$, and $l_1 = l_4 = 10.74$, $s_2 = s_3 = 1.3$, and $l_2 = l_3 = 10.72$.

III. FILTER DESIGN

A. INLINE TOPOLOGY

For demonstration, a fourth-order waveguide BPF based on the proposed slotted resonator is designed. The filter is firstly designed in an inline topology as shown in Fig. 5(a).

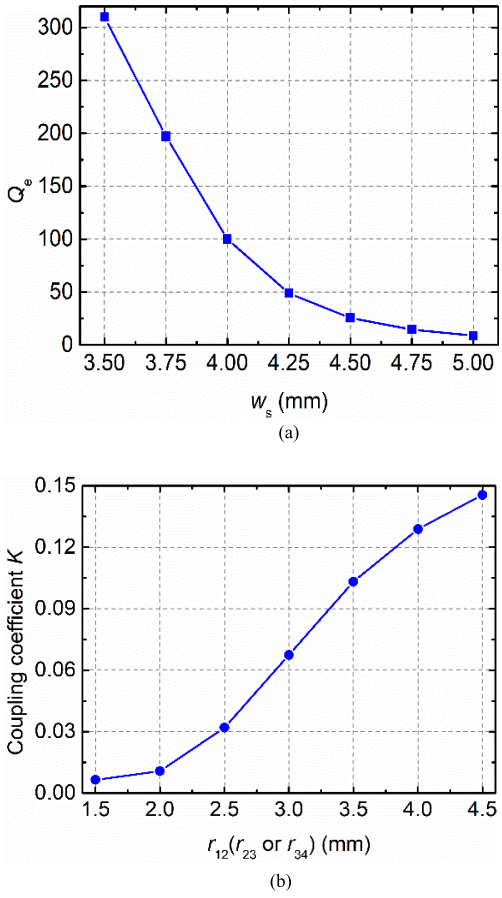

FIGURE 6. Extracted Q_e, K_{12} (= K_{34}) and K_{23} values from EM simulation. (a) Q_e versus w_s. (b) K_{12} (= K_{34}) or K_{23} versus r_{12}/r_{34}.or r_{23}.

It consists of four coupled slotted spherical resonators with input and output feed waveguides. The filter is designed with center frequency of 31 GHz, bandwidth of 880 MHz, and passband return loss (RL) of 20 dB. Based on the coupling matrix approach [22], the required denormalized external quality factors and coupling coefficients are obtained as $Q_{eS} = Q_{eL} = 32.87$, $K_{12} = K_{34} = 0.0258$, and $K_{23} = 0.0198$. The external quality factors Q_{eS}/Q_{eL} can be adjusted by the aperture width w_s as shown in Fig. 5(b). The inter-resonator coupling coefficients K_{12}/K_{34} and K_{23} can be controlled by the radius r_{12}/r_{34} and r_{23}, respectively, as shown in Fig. 5(c). Figs. 6(a) and 6(b) plot the extracted external quality factors and inter-resonator coupling coefficients against the aperture width w_s and the radius of the coupling iris, respectively. The initial dimensions of the filter can be obtained from Fig. 6. It should be noted that enlarging the slot dimensions not only improves the suppression level of spurious passbands, but also increase the in-band insertion loss of the filter due to the decreased Q_u of the TM_{211} mode. Therefore, the slots dimensions should be carefully selected to obtain a balance between the in-band insertion loss and the suppression level. The dimensions of the filter after optimization are given in the caption of Fig. 5.

Fig. 7 shows the simulated frequency responses of the slotted filter in comparison with that of the unslotted filter.

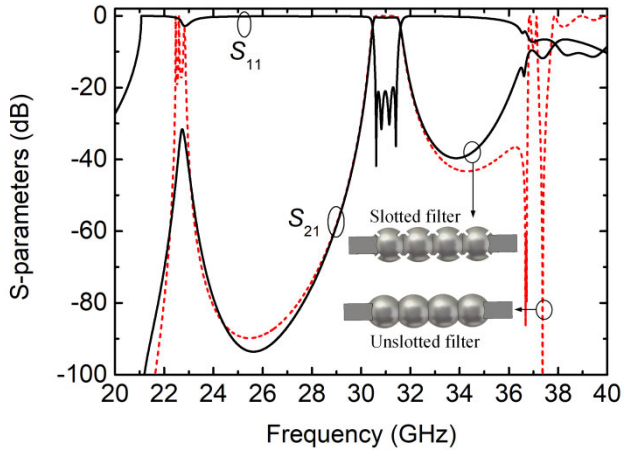

FIGURE 7. EM-simulated frequency responses of the unslotted and slotted BPFs arranged in inline topology.

It can be seen that the spurious passband constituted by TM_{101} mode at 22.65 GHz is well suppressed, but the suppression level on the spurious passbands constituted by TE_{101} and TM_{311} modes at 36.97 and 38.96 GHz is poor. To improve this, a new BPF arranged in "Z" topology is proposed in the following section to achieve a better spurious suppression stopband without enlarging the slots dimensions significantly.

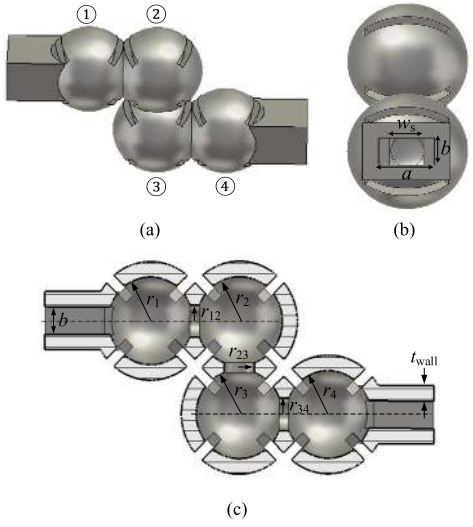

FIGURE 8. Illustration of the Z-shaped fourth-order Ka-band BPF. (a) A 3-D view. (b) A side view (c) cross section view. Critical dimensions of the filter in millimeters are $a = 7.112$, $b = 3.556$, $w_S = 4.58$, $r_1 = r_4 = 5.68$, $r_2 = r_3 = 5.77$, $r_{12} = r_{34} = 2.12$, $r_{23} = 2.03$, $t_{wall} = 2$. The slot dimensions of the resonators (s_i and l_i denoted in Fig. 1(a), $i = 1, 2, 3,$ and 4 for the i^{th} resonator) are $s_1 = s_4 = 1.3$, and $l_1 = l_4 = 10.73$, $s_2 = s_3 = 1.3$, and $l_2 = l_3 = 11.04$.

B. "Z" TOPOLOGY

The "Z" topology is shown in Fig. 8, where the resonator 1 and resonator 2 as well as the resonator 3 and resonator 4 are coupled horizontally, and the resonator 2 and resonator 3 are

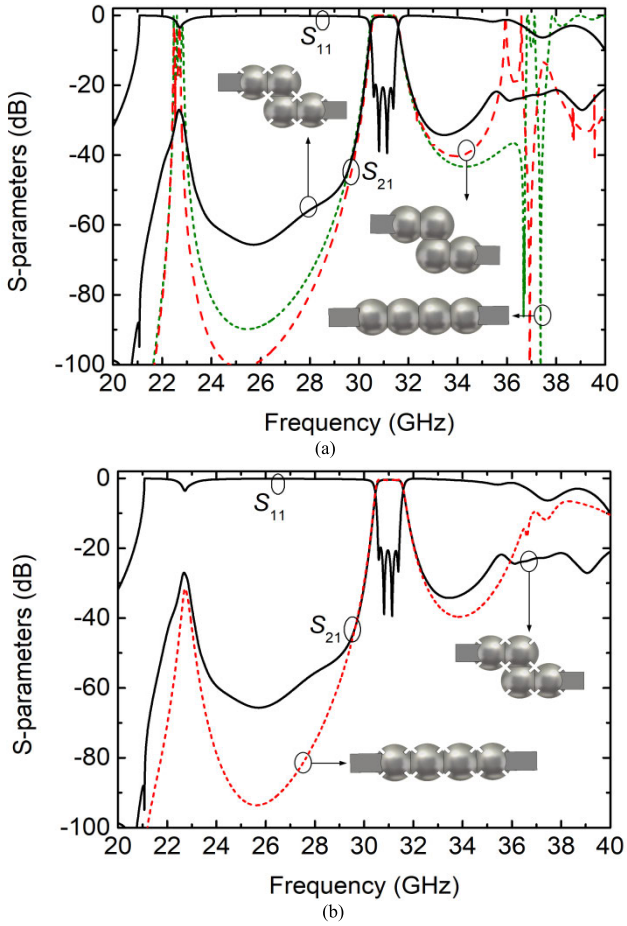

FIGURE 9. (a) EM-simulated frequency responses of the unslotted BPFs with inline topology and "Z" topology and slotted BPFs arranged in "Z" topology. (b) EM-simulated frequency responses of the slotted BPFs arranged in inline topology and "Z" topology.

coupled vertically. Referring to Fig. 1(d), the current density on the top and bottom of the spherical resonator at TM_{311} mode is small. Therefore, the "Z" topology can decrease the coupling strength of the spurious passband constituted by the TM_{311} mode. To illustrate the concept, Fig. 9(a) compares the frequency responses of the unslotted BPFs arranged in inline topology and "Z" topology and the slotted BPF arranged in "Z" topology with the same passband specifications. It is found that the TM_{311}-mode spurious passband at 38.96 GHz of the unslotted BPF arranged in "Z" topology (denoted with red dash line) has been suppressed effectively. Meanwhile, due to the influence of the suppressed TM_{311}-mode spurious passband, the TE_{101}-mode spurious passband is shifted slightly. With further introduction of slots on the unslotted "Z" topology BPF, the slotted BPF achieves an enhanced spurious suppression stopband. Furthermore, Fig. 9(b) shows the simulated results of the slotted "Z" topology BPF compared with that of the slotted inline topology. As it can be seen, the proposed "Z" topology BPF improves the suppression level by around 13.5 dB compared with the slotted inline filter. The optimized dimensions of the proposed filter are shown in the caption of Fig. 8.

C. TOLERANCE ANALYSIS

The tolerance analysis is utilized to determine the sensitivity of the filter frequency response with reduced dimensional tolerances as a result of the fabrication. As mentioned in the introduction, the volume of TM_{211}-mode spherical resonator (i.e., 882 mm^3, working at 31 GHz) is larger than that of the TM_{101}-mode resonator (i.e., 310 mm^3), giving the filter a better tolerance to fabrication errors at high frequencies. Here, a tolerance analysis is performed to show the advantage of the Z-shaped slotted filter over the conventional TM_{101}-mode spherical resonator BPF in terms of better tolerance performance.

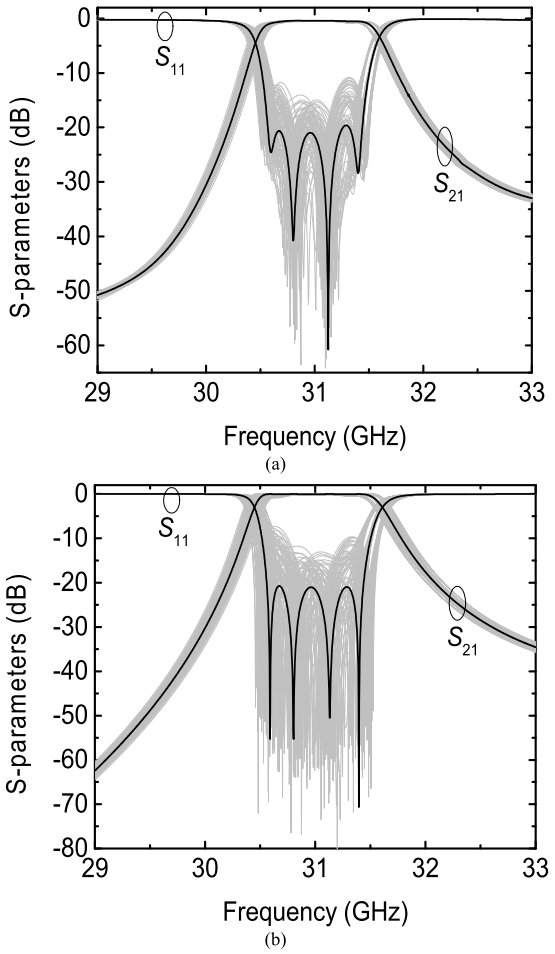

FIGURE 10. Sensitivity analysis to fabrication tolerances (±10 μm) of (a) the slotted "Z" topology BPF. (b) the TM_{101}-mode spherical resonator BPF with inline topology. Black solid lines: original optimized responses; Gray lines: tolerance responses.

One hundred simulations using randomly varied filter dimensions with a tolerance of ±10 μm are carried out. Figs. 10(a) and 10(b) show the resultant responses (grey lines) against the original optimized one (black solid lines) for the Z-shaped slotted BPF and conventional TM_{101}-mode spherical resonator filter, respectively. As expected, the results indicate that the high-order mode Z-topology filter is less sensitive to dimensional changes than the conventional fundamental mode filter. The return loss of the proposed filter drops from 20 to 10 dB in the worst case. Whereas the conventional one, deteriorates from 20 to 7 dB. In addition,

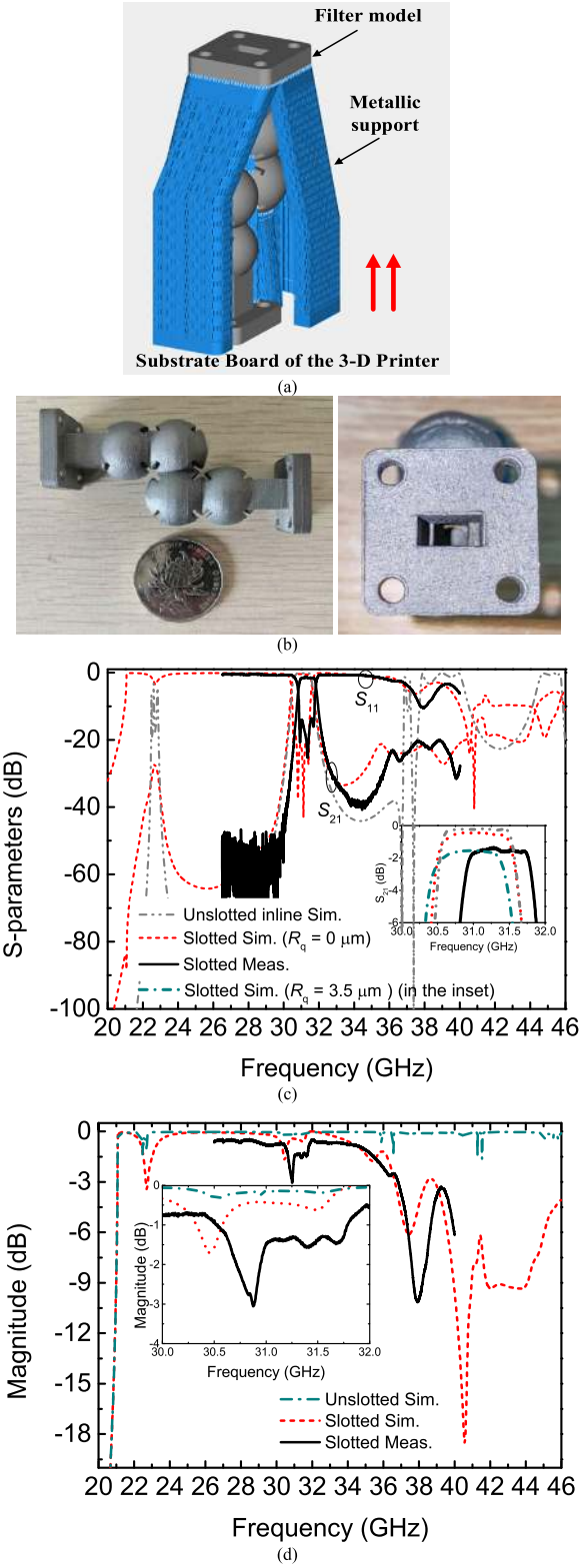

FIGURE 11. (a) Illustration of the printing orientation of the BPF model with the red arrows indicating the printing direction. (b) Fabricated filter (left: A top view; right: A view from waveguide). (c) The frequency performance. (d) The loss factor $(1 - |S_{11}|^2 - |S_{21}|^2)$.

TABLE 2. Comparison with some reported 3-D printed BPFs.

Ref.	Manufacturing techniques.	f_0 (GHz)	FBW (%)	IL (dB)	Δf (%)	Spurious Suppression	Measured Q_u	Size (mm^3)
[3]	SLM	12.875/14.125	1.94/1.77	0.2	<0.2	Yes (>55 dB)	4300/4600	N/A
[8]	SLA	107.2	6.3	0.95	7.2	—	152	2.5×1.25×9
[9]	SLM	75.5	5.3	8	2.7	—	281	3.1×1.5×36
[10]	SLS	12.5	4	—	1.8	—	N/A	N/A
[11]	MLS	88.34/89.1	12.1/11.07	1.94/1	1.84/1	—	120/255	N/A
[14]	SLA	10	5	0.11	0.05	—	5270	120×51×55
[15]	SLA	10	3	0.24	<0.01	—	N/A	76×30×31
[20]	SLM	10.9	3	0.9	<0.9	Yes (>34 dB)	734	N/A
[21]	SLA/SLM	10	1	0.2/0.33	0.04/0.5	Yes (>20 dB)	6094/4060	120×40×40/ 105×40×40
T.W.	SLM	31	2.84	1.53	1.1	Yes (>20 dB)	493	61×19×19

*T.W.: This work. Ref [10] is a butler matric with filtering function. N/A: not available.

the proposed filter exhibits smaller passband shift and bandwidth variation. Therefore, the high-order mode slotted filter offers a better tolerance, and thus easier fabrication can be gained.

IV. FABRICATION, MEASUREMENT, AND DISCUSSION

The complex geometry of the filter would normally require time-consuming CNC milling in a split-block form and then assembly using screws. Here, a metal-based SLM 3-D printing technique was employed to produce the filter in a monolithic form without requiring any assembly. The filter was printed with an aluminum-silicon-based alloy AlSi10Mg (89 weight percent (wt. %) aluminum, 9.5 wt. % silicon, and 1.5 wt. % others) in a powder form with particle sizes ranging from 15 to 53 μm. The printing orientation for the filter is illustrated in Fig. 11(a), Due to the self-supporting capability of the spherical shaped resonators, no supporting structures are required inside the cavity filter. The metallic supports for the slots and outside the filter can be manually removed with little effect on the microwave performance. A chemical polishing process was utilized to reduce the surface roughness of the printed device. Fig. 11(b) shows photographs of the fabricated filter. The measurement was carried out by Agilent Vector Network Analyzer E8362C. Since the *Ka*-to-*K*-band and *Ka*-to-*U*-band waveguide tapers were not available, the frequency responses at *K*-band (18-26.5 GHz) and *U*-band (40-60 GHz) were not measured. Here we give the measured results at *Ka*-band. The measured frequency responses compared with simulations are shown in Fig. 11(c), showing a good agreement. The measured average passband insertion loss (IL) is 1.53 dB in comparison with the simulated IL of 0.46 dB (based on an ideal electrical conductivity of 3.56×10^7 S/m for aluminum). Assuming the increased IL is solely due to the surface roughness of the printed filter, this would mean an equivalent root square roughness (R_q) of 3.5 μm (shown in the inset of Fig. 11(c)). However, the aluminum is not perfect so this is an upper limit. Assuming the increased IL is solely due to the electrical conductivity of the printed filter, the effective electrical conductivity of the filter was fitted as 1.2×10^6 S/m from the measured in-band IL in CST Studio Suite, which is much lower than that of the aluminum ($=3.56 \times 10^7$ S/m). In addition, from the inset, the simulated average ILs of the unslotted and slotted filters are 0.23 dB and 0.46 dB, respectively. The IL difference is 0.23 dB, which is very small and corresponds to the radiation loss. Due to the relatively low metal electrical conductivity and high surface roughness, the measured Q_u of the slotted resonator is about 493 using the estimation method described in [22]. The measured Q_u of the proposed filter can be significantly improved by using the SLA 3-D printing process, which offers higher electrical conductivity and lower surface roughness as demonstrated in our previous work [21]. The measured return loss (RL) is better than 13.6 dB. The measured frequency shift (Δf) and bandwidth are 1.1% (341 MHz) and 822 MHz, respectively. This is induced mainly by shrinkage of the printed coupling irises and resonators [24], which can be compensated for by offsetting the filter dimensions in the CAD design before fabrication. In addition, the filter shows a 20-dB spurious suppression stopband up to 40.9 GHz as predicted by the simulation and a 13.5-dB spurious suppression stopband up to 44.2 GHz, with the spurious passbands at around 22.65, 36.97 and 38.96 GHz suppressed. From the simulation, the first spurious passband appears beyond 44.3 GHz. It should be mentioned that a higher order slotted spherical resonator filter or an additional band notch structure can be employed to increase the rejection level of the lower and upper stopband.

It should be noted that radiation occurs in the lower and upper stopband, which can be quantified by the loss factor $(1 - |S_{11}|^2 - |S_{21}|^2)$ of the filter, as demonstrated in Fig. 11(d). Strong radiation of the spurious modes is evident; the frequencies at lower and upper stopband with the maximum loss of the loss factor $(1 - |S_{11}|^2 - |S_{21}|^2)$ are 22.7 and 40.6 GHz, while within the passband the simulated insertion-loss difference between the unslotted and slotted filters is less than 0.23 dB, corresponding to the radiation loss. Therefore, the slots introduce negligible radiation within the passband, but strong radiation of the spurious modes at the lower and upper stopband. Note that due to the slots introducing negligible radiation within the passband, any coupling effect between two adjacent slots/resonators at frequencies within the passband is also insignificant.

The potential interference due to the radiation to external circuits can be alleviated by covering the slots with absorbing materials. The passband and stopband measurement results of the filter with the absorbing materials show no significant difference from the ones in Figs. 11(c) and 11(d). Finally, a comparison of the proposed filter to previous related work is summarized in Table 2.

V. CONCLUSION

A TM_{211}-mode slotted spherical resonator has been presented in this article. Benefiting from the slots, the fundamental TM_{101} and two higher spurious modes (TE_{101} and TM_{311}) can be rejected without decreasing the Q_u of the TM_{211} mode significantly. In addition, A Z-shaped topology is proposed for the filter to achieve better spurious suppression by decreasing the coupling strength of the spurious TM_{311} mode. A prototype filter has been manufactured by SLM 3-D printing process to verify the proposed idea. The presented slotted resonator filter offers a 20-dB spurious suppression stopband up to 40.9 GHz. It is worth mentioning that the monolithic building of the filter offers a major advantage for high power applications.

REFERENCES

[1] S. Amari, "Application of representation theory to dual-mode microwave bandpass filters," *IEEE Trans. Microw. Theory Techn.*, vol. 57, no. 2, pp. 430–441, Feb. 2009.

[2] R. J. Cameron and J. D. Rhodes, "Asymmetric realizations for dual-mode bandpass filters," *IEEE Trans. Microw. Theory Techn.*, vol. 29, no. 1, pp. 51–58, Jan. 1981.

[3] P. Booth and E. V. Lluch, "Enhancing the performance of waveguide filters using additive manufacturing," *Proc. IEEE*, vol. 105, no. 4, pp. 613–619, Apr. 2017.

[4] Y. Zhang, F. Zhang, Y. Gao, J. Xu, C. Guo, and X. Shang, "3D printed waveguide step-twist with bandpass filtering functionality," *Electron. Lett.*, vol. 56, no. 11, pp. 527–528, May 2020.

[5] O. A. Peverini, M. Lumia, G. Addamo, F. Paonessa, G. Virone, R. Tascone, F. Calignano, G. Cattano, and D. Manfredi, "Integration of an *H* -Plane bend, a twist, and a filter in Ku/K-band through additive manufacturing," *IEEE Trans. Microw. Theory Techn.*, vol. 66, no. 5, pp. 2210–2219, May 2018.

[6] C. Tomassoni, G. Venanzoni, M. Dionigi, and R. Sorrentino, "Compact quasi-elliptic filters with mushroom-shaped resonators manufactured with 3-D printer," *IEEE Trans. Microw. Theory Techn.*, vol. 66, no. 8, pp. 3579–3588, Aug. 2018.

[7] C. Guo, J. Li, D. D. Dinh, X. Shang, M. J. Lancaster, and J. Xu, "Ceramic filled resin based 3D printed X-band dual-mode bandpass filter with enhanced thermal handling capability," *Electron. Lett.*, vol. 52, no. 23, pp. 1929–1931, Nov. 2016.

[8] M. D'Auria, W. J. Otter, J. Hazell, B. T. W. Gillatt, C. Long-Collins, N. M. Ridler, and S. Lucyszyn, "3-D printed metal-pipe rectangular waveguides," *IEEE Trans. Compon., Packag., Manuf., Technol.*, vol. 5, no. 9, pp. 1339–1349, Sep. 2015.

[9] B. Zhang and H. Zirath, "3D printed iris bandpass filters for millimetre-wave applications," *Electron. Lett.*, vol. 51, no. 22, pp. 1791–1793, Oct. 2015.

[10] V. Tornielli di Crestvolant, P. Martin Iglesias, and M. J. Lancaster, "Advanced butler matrices with integrated bandpass filter functions," *IEEE Trans. Microw. Theory Techn.*, vol. 63, no. 10, pp. 3433–3444, Oct. 2015.

[11] M. Salek, X. Shang, R. C. Roberts, M. J. Lancaster, F. Boettcher, D. Weber, and T. Starke, "W-band waveguide bandpass filters fabricated by micro laser sintering," *IEEE Trans. Circuits Syst. II, Exp. Briefs*, vol. 66, no. 1, pp. 61–65, Jan. 2019.

[12] B. Zhang and H. Zirath, "A metallic 3-D printed E-band radio front end," *IEEE Microw. Wireless Compon. Lett.*, vol. 26, no. 5, pp. 331–333, May 2016.

[13] O. A. Peverini, G. Addamo, M. Lumia, G. Virone, F. Calignano, M. Lorusso, and D. Manfredi, "Additive manufacturing of Ku/K-band waveguide filters: A comparative analysis among selective-laser melting and stereo-lithography," *IET Microw., Antennas Propag.*, vol. 11, no. 14, pp. 1936–1942, Nov. 2017.

[14] C. Guo, X. Shang, M. J. Lancaster, and J. Xu, "A 3-D printed lightweight X-band waveguide filter based on spherical resonators," *IEEE Microw. Wireless Compon. Lett.*, vol. 25, no. 7, pp. 442–444, Jul. 2015.

[15] C. Guo, X. Shang, J. Li, F. Zhang, M. J. Lancaster, and J. Xu, "A lightweight 3-D printed *X*-band bandpass filter based on spherical dual-mode resonators," *IEEE Microw. Wireless Compon. Lett.*, vol. 26, no. 8, pp. 568–570, Aug. 2016.

[16] Y. Li, J. Li, M. Zhang, H. Wang, J. Xu, and S. Xiao, "A monolithic stereolithography 3-D printed Ka-band spherical resonator bandpass filter," in *Proc. IEEE Radio Wireless Symp. (RWS)*, Anaheim, CA, USA, Jan. 2018, pp. 56–59.

[17] J. Li, C. Guo, L. Mao, and J. Xu, "Compact high-Q hemispherical resonators for 3-D printed bandpass filter applications," in *IEEE MTT-S Int. Microw. Symp. Dig.*, Honolulu, HI, USA, Jun. 2017, pp. 1591–1594.

[18] J. Li, C. Guo, L. Mao, and J. Xu, "3D printed bandpass filters using compact high-Q hemispherical resonators with improved out-of-band rejection," *Electron. Lett.*, vol. 53, no. 6, pp. 413–415, Mar. 2017.

[19] J. Li, C. Guo, L. Mao, J. Xiang, G.-L. Huang, and T. Yuan, "Monolithically 3-D printed hemispherical resonator waveguide filters with improved out-of-band rejections," *IEEE Access*, vol. 6, pp. 57030–57048, Oct. 2018.

[20] J. Li, S. Li, G.-L. Huang, T. Yuan, and M. M. Attallah, "Monolithic 3D-printed slotted hemisphere resonator bandpass filter with extended spurious-free stopband," *Electron. Lett.*, vol. 55, no. 6, pp. 331–333, Mar. 2019.

[21] F. Zhang, S. Gao, J. Li, Y. Yu, C. Guo, S. Li, M. Attallah, X. Shang, Y. Wang, M. J. Lancaster, and J. Xu, "3-D printed slotted spherical resonator bandpass filters with spurious suppression," *IEEE Access*, vol. 7, pp. 128026–128034, Sep. 2019.

[22] J. S. Hong and M. J. Lancaster, *Microstrip Filters for RF/Microwave Applications*. New York, NY, USA: Wiley, 2001.

[23] USA. (Jul. 2018). *CST Computer Simulation Technology AG*. [Online]. Available: https://www.cst.com

[24] H. H. Zhu, L. Lu, and J. Y. Fuh, "Study on shrinkage behavior of direct laser sintering metallic powder," *Proc. Inst. Mech. Eng. B, J. Eng. Manuf.*, vol. 220, no. 2, pp. 183–190, Feb. 2006.

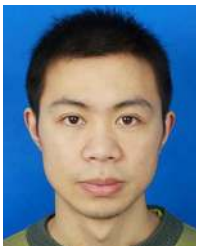

FAN ZHANG (Member, IEEE) was born in Sichuan, China. He is currently pursuing the Ph.D. degree in radio physics with the School of Physics, University of Electronic Science and Technology of China, Chengdu, China.

From 2017 to 2018, he was a Visiting Student with the University of Birmingham, Birmingham, U.K. His current research interests include microstrip multi-band bandpass filters, electrically tunable planar filters, RF-MEMS devices, 3-D printed waveguide components, and millimeter-wave circuits.

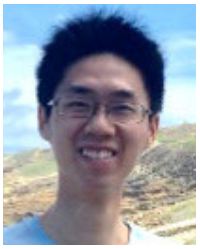

CHENG GUO was born in Chengdu, China, in 1990. He received the B.E. degree in communication engineering from Southwest Jiaotong University (Emei), Chengdu, in 2012, and the Ph.D. degree in radio physics from the University of Electronic Science and Technology of China, Chengdu, in 2016.

From 2014 to 2016, he was a Visiting Ph.D. Student with the University of Birmingham, Birmingham, U.K., where he was a Research Fellow, from 2017 to 2018. He is currently an Associate Professor with the School of Information and Communications Engineering, Xi'an Jiaotong University, Xi'an, Shaanxi, China. His current research interests include 3-D printed passive microwave devices, schottky diode-based THz frequency multipliers and mixers, and micromachined millimeter-wave/THz circuits.

Dr. Guo was a co-recipient of the IEEE Microwave Theory and Techniques Society Tatsuo Itoh Award in 2017.

YI ZHANG (Student Member, IEEE) was born in Sichuan, China. He received the B.S. degree in physics from Sichuan Normal University, Chengdu, China, in 2016. He is currently pursuing the Ph.D. degree in radio physics with the School of Physics, University of Electronic Science and Technology of China, Chengdu. His current research interests include 3-D printing of passive microwave circuits and antenna.

YANG GAO (Member, IEEE) received the B.Eng. degree in telecommunication engineering from the Beijing Institute of Technology, Beijing, China, in 2014, and the Ph.D. degree in microwave engineering from the University of Birmingham, Birmingham, U.K., in 2018. After graduating from the University of Birmingham, he joined Zhengzhou University, Zhengzhou, China, as a Lecturer. In 2019, he was employed by the Department of International Cooperation, Ministry of Science and Technology of China on secondment. He is also an Honorary Research Fellow with the Emerging Device Technology Group, University of Birmingham. His current research interests include integrated microwave-terahertz circuits, and passive and active components.

BING LIU was born in Anhui, China. He received the B.E. degree in electronic science and technology from Anhui Science and Technology University, Anhui, and the M.S. degree in radio physics from the School of Physics, University of Electronic Science and Technology of China, Chengdu, China, where he is currently pursuing the Ph.D. degree in physics. His current research interests include design of microwave filters and filtering antenna.

MINJIE SHU received the B.Eng. degree in information engineering from Xi'an Jiaotong University, Xi'an, China, in 2014, where he is currently pursuing the Ph.D. degree in electronics science and technology. His research interest includes the design of micromachined millimeter wave components.

YI WANG (Senior Member, IEEE) was born in Shandong, China. He received the B.Sc. degree in physics and the M.Sc. degree in condensed matter physics from the University of Science and Technology, Beijing, China, in 1998 and 2001, respectively, and the Ph.D. degree in electronic and electrical engineering from the University of Birmingham, Birmingham, U.K., in 2005.

In 2011, he became a Senior Lecturer and then a Reader with the University of Greenwich. In 2018, he joined the University of Birmingham as a Senior Lecturer. His current research interests include millimeter-wave and terahertz devices for metrology, communications and sensors, micromachining, microwave circuits based on multiport filtering networks, and filter-antenna integration.

YULIANG DONG was born in Sichuan, China, in 1972. He received the bachelor's degree in electronic engineering from Northwestern Polytechnical University, Xi'an, China, in 1993, and the Ph.D. degree in electromagnetic field and microwave technology from Beihang University, Beijing, in 2005. He is currently a Professor with Chengdu Aeronautic Polytechnic, China. His research interests include microwave circuits, passive components, antennas, and microwave CAD technology.

MICHAEL J. LANCASTER (Senior Member, IEEE) was born in U.K., in 1958. He received the degree in physics and the Ph.D. degree for research into non-linear underwater acoustics from Bath University, U.K., in 1980 and 1984, respectively.

After leaving Bath University, he joined the Surface Acoustic Wave (SAW) Group, Department of Engineering Science, Oxford University, as a Research Fellow. The research was in the design of new, novel SAW devices, including RF filters and filter banks. In 1987, he became a Lecturer with the Department of Electronic and Electrical Engineering, University of Birmingham, lecturing in electromagnetic theory and microwave engineering. Shortly after he joined the department, he began the study of the science and applications of high temperature superconductors, working mainly at microwave frequencies. He was promoted to the Head of the Emerging Device Technology Research Center, in 2000, and the Head the Department of Electronic, Electrical and Computer Engineering, University of Birmingham, in 2003. He has published two books and more than 170 articles in refereed journals. His current research interests include microwave filters and antennas, and the high-frequency properties and applications of a number of novel and diverse materials.

Dr. Lancaster is a Fellow of the IET and the U.K. Institute of Physics. He is a Chartered Engineer and a Chartered Physicist. He has served on the IEEE Microwave Theory and Techniques International Microwave Symposium Technical Program Committee.

JUN XU was born in Chengdu, China, in 1963. He received the B.S. and M.S. degrees from the University of Electronic Science and Technology of China (UESTC), Chengdu, in 1984 and 1990, respectively.

In 1997, he became an Associate Professor with UESTC, where he was promoted as a Professor in 2000. He is currently the Head of the School of Physics, UESTC. His main research interests include microwave theory and technology, millimeter-wave hybrid integrated technology, millimeter-wave communication and radar radio frequency technology, and 3-D printing of passive microwave devices.